HHS Public Access

Author manuscript

NanoImpact. Author manuscript; available in PMC 2019 May 13.

Published in final edited form as:

NanoImpact. 2019 January ; 13: 13–25. doi:10.1016/j.impact.2018.11.002.

Development of a standardized food model for studying the impact of food matrix effects on the gastrointestinal fate and toxicity of ingested nanomaterials

Zipei Zhang[a,1], **Ruojie Zhang**[a,1], **Hang Xiao**[a], **Kunal Bhattacharya**[b], **Dimitrios Bitounis**[b], **Philip Demokritou**[b,*], and **David Julian McClements**[a,b,*]

[a]Department of Food Science, University of Massachusetts, Amherst, MA 01003, USA

[b]Center for Nanotechnology and Nanotoxicology, Department of Environmental Health, Harvard T. H. Chan School of Public Health, Boston, MA 02115, USA

Abstract

Food matrix effects impact the bioavailability and toxicity of pharmaceuticals, nutraceuticals, pesticides, and engineered nanomaterials (ENMs). However, there are currently no standardized food models to test the impact of food matrix effects using *in vitro* gastrointestinal models. The purpose of this study was to establish a *standardized food model* (SFM) for evaluating the toxicity and fate of ingested ENMs and then to assess its efficacy by examining the impact of food matrix effects on the toxicity of TiO_2 nanoparticles. The formulation of the SFM was based on the average composition of the US diet: 3.4% protein (sodium caseinate); 4.6% sugar (sucrose); 5.2% digestible carbohydrates (modified corn starch); 0.7% dietary fiber (pectin); 3.4% fat (corn oil); and, 0.5% minerals (sodium chloride). The SFM consisted of an oil-in-water emulsion suitable for use in both wet and dried forms. The dried form was produced by spray drying the emulsion to improve its handling and extend its shelf-life. The particle size (D_{32} = 135 nm), surface charge (−37.8 mV), viscosity, color (L^*, a^*, b^* = 82.1, −2.5, 1.3), and microstructure of the wet SFM were characterized. The hydration properties, flowability (repose angle ≈ 27.9°; slide angle ≈ 28.2°), and moisture sorption isotherms of the dry SFM were comparable to commercial food powders. The potential gastrointestinal fate of the SFM was determined using a simulated gastrointestinal tract, including mouth, stomach, and small intestine steps. Conversion of the SFM into a powdered form did not impact its gastrointestinal fate. A nanotoxicology case study with TiO_2 nanoparticles exposed to a tri-culture epithelial cell model showed that food matrix effects reduced ENM cytotoxicity more than 5-fold. The SFM developed in the current study could facilitate studies of the impact of food matrix effects on the gastrointestinal fate and toxicity of various types of food NPs.

[*]*Corresponding authors:* D.J. McClements, Department of Food Science, University of Massachusetts, Amherst, MA 01003, USA. Tel.: +1 413-545-2275; fax: +1 413-545-1262; mcclements@foodsci.umass.edu, P. Demokritou, *Center for Nanotechnology and Nanotoxicology, Department of Environmental Health, Harvard T. H. Chan School of Public Health, Boston, MA 02115, USA*, pdemokri@hsph.harvard.edu.

[1]These authors contributed equally to the present work.

Keywords

food matrix; nanoparticle; standard food model; bioavailability; digestion

1. Introduction

Nanotechnology is used in a range of non-food consumer products to achieve specific functional effects, such as in printer toners (Pirela, et al., 2016; Pirela, et al., 2014). In the food and agriculture industry, current and potential applications of inorganic engineered nanoparticles (NPs) aim to improve food quality (Pyrgiotakis, et al., 2014), sensory appeal, shelf life, and safety (Eleftheriadou, Pyrgiotakis, & Demokritou, 2017; Smolkova, El Yamani, Collins, Gutleb, & Dusinska, 2015) and even increase food production (Servin & White, 2016). For example, titanium dioxide NPs are used to increase whiteness (Weir, Westerhoff, Fabricius, Hristovski, & Von Goetz, 2012), silver NPs are used as antimicrobials (Sekhon, 2010), silicon dioxide NPs are used as anticaking agents (Peters, et al., 2016), zinc oxide NPs are used as nutritional supplements (Mura, Seddaiu, Bacchini, Roggero, & Greppi, 2013), and nanocellulose fibers can be used to reduce fat bioavailability (DeLoid, et al., 2018). Engineered nanomaterials (ENMs) may be intentionally added to food products or they may unintentionally get into them *e.g.,* by leaching from packaging materials (McClements & Xiao, 2017). Consequently, inorganic and organic engineered NPs may be ingested by humans and pass through the gastrointestinal tract (GIT).

The properties of ENMs change appreciably when their dimensions are reduced into the nanoscale, which means that it is important to establish their safety profiles (Jain, Ranjan, Dasgupta, & Ramalingam, 2018; Kaphle, Navya, Umapathi, & Daima, 2018). Several studies suggest that certain types of nanoparticles have a pathogenic potential. For example, nanoparticles emitted by printers induce epigenetic alterations in mice (Lu, et al., 2016) while others can cause aberrant changes in the proteome (Ahluwalia, et al., 2013; Georgantzopoulou, 2015). Moreover, several metal and metal oxides cause genotoxicity and cytotoxicity in cell lines cultured *in vitro*, induce oxidative stress, and immunotoxicity (Jain, et al., 2018; Singh & Nalwa, 2007). The properties and biological effects of nanoparticles have a dynamic relationship with their immediate environment (Gao & Lowry, 2017). For instance, ingested nanomaterials may pass through the upper GIT and reach the colon where they might alter the composition of the gut microbiome, which could have an indirect impact on human health (Bouwmeester, van der Zande, & Jepson, 2018). The potentially adverse effects of ingested ENMs may therefore occur within the GIT itself, as well as in other organs in the body after absorption.

There is increasing appreciation of the importance of food matrix effects on the gastrointestinal fate and potential toxicity of ingested NPs (DeLoid, et al., 2017b; Ramos, Ramos, & Gómez-Gómez, 2017; Šimon & Joner, 2008; Zhang, et al., 2018). The food matrix contains a variety of molecular and colloidal species that can interact with ENMs and alter their GIT fate. In particular, the nature of ingested foods impacts the composition and structure of the gastrointestinal fluids surrounding the NPs, which influences properties such as their solubility, surface composition, electrical charge, and aggregation state

(McClements, et al., 2016; McClements, et al., 2017). As a result, the gastrointestinal fate and potential toxicity of NPs may be strongly influenced by food matrix effects. Indeed, the potential impact of food matrix effects have been highlighted in several recent studies (Cao, et al., 2016; Lichtenstein, et al., 2015; McClements, et al., 2016; Walczak, et al., 2015). Thus, knowledge of food matrix effects is critical for understanding the gastrointestinal fate of food ENMs and conducting potential risk assessment.

At present, studies on the toxicity of ingested nanomaterials lack methodological standardization (Sohal, O'Fallon, Gaines, Demokritou, & Bello, 2018). Deloid et al. recently presented an integrated methodology for assessing the impact of food matrix and gastrointestinal effects on the biokinetics and cellular toxicity of ingested engineered nanomaterials (DeLoid, et al., 2017c). One of the challenges in establishing the potential impact of food matrix effects on the gastrointestinal fate and bioactivity of NPs is that ingested foods vary widely in their compositions and structures. Ideally, there is a need for a standardized food model that can be used by different researchers so that results can be reliably compared between different laboratories. This would allow a rapid assessment of the relative importance of food matrix effects for different kinds of nanoparticles, thereby allowing for a more accurate hazard assessment. Given the growing body of work suggesting that ENMs are subject to physicochemical transformations within the GIT, the purpose of our research was to establish a *standardized food model* (SFM) that could be used for evaluating the impact of food matrix effects on ingested ENMS as well as their biokinetics and potential toxicity.

The composition of our SFM was based on the composition of the typical US diet. The diet used is the average for men and women of 20 years or older and was taken from the "What We Eat in America" NHANES 2013–2014 database. This food survey reports the total nutrient intake for men and women of different ages. It has values for typical amounts of protein, fat, dietary fiber, carbohydrates, and minerals consumed each day, which can be used to develop a standardized model of the typical American diet. Therefore, the SFM was prepared based on the composition and proportions of these listed nutrients.

The colloidal properties of SFM, including particle size, surface charge, and microstructure, were measured because they will impact its interactions with ENMs. Its behavior within a commonly utilized simulated gastrointestinal model (mouth, stomach, and small intestine) was also determined. To increase its versatility and shelf-life, the SFM was converted into a powdered form using spray drying. As a demonstration of its applicability in nanotoxicology, the powdered SFM was reconstituted and utilized in a cellular toxicity study of ingested TiO_2 nanoparticles. Overall, the availability of this SFM should facilitate studies on the impact of food matrix effects on the gastrointestinal fate and toxicity of ingested ENMs. It must be noted, that this food model may also be applied in other studies where food matrix effects are important, such as the bioavailability of pharmaceuticals, nutraceuticals, or pesticides, which will be the focus of our future research.

2. Materials and Methods

2.1. Materials

Corn oil was purchased from a local food supplier and stored at 4°C prior to use. The following chemicals were purchased from the Sigma Chemical Company (Sigma Chemical Co., St Louis, MO): mucin from porcine stomach; α-amylase (782.14 units/mg protein), pepsin from porcine gastric mucosa (250 units per mg); pancreatin (100–400 units per mg protein); porcine bile extract; and, Nile red. Powdered sodium caseinate was purchased from the American Casein Company (MP Biomedicals LLC). Modified food starch (Instant Pure-Cote B792) was purchased from the Grain Processing Corporation (Muscatine, IA). Pectin (1400) was supplied by TIC GUMs (White Marsh, MD). Sucrose and sodium chloride were purchased from the Fisher Chemical Company (Pittsburgh, PA). All chemicals were of analytical grade. All solutions were prepared using double distilled water obtained from a water purification system (Nanopure Infinity, Barnstead International, Dubuque, IA).

2.2. Standardized food model formation and characterization

The preparation of the SFM was based on the reported nutrient composition of the typical US diet (www.ars.usda.gov/nea/bhnrc/fsrg). A summary of the nutrients incorporated into the SFM formulation developed in our study is shown in Table 1. Sodium caseinate (1%, w/w), used as a representative food protein, was dissolved in phosphate buffer solution (10 mM, pH 7) at ambient temperature with continual stirring for 2 hours to ensure full dissolution. The dissolved caseinate solution was then subjected to filtration to remove any small amounts of undissolved powder particles (removal of this material did not significantly change the final protein concentration). Corn oil (7.64%, w/w), a representative food fat, was then added to the sodium caseinate solution and blended using a high-shear mixer for 2 minutes at high speed. The resulting coarse emulsion was passed through a high-pressure homogenizer (M110Y, Microfluidics, Newton, MA) with a 75 μm interaction chamber (F20Y) at 12,000 psi for 3 passes to create a fine emulsion. Additional sodium caseinate powder was then slowly added into the fine emulsion (final protein concentration = 7.68% w/w) with continual stirring until the protein was fully dissolved (around 30 min). The other food components were sequentially added into the emulsion phase in the following order to reach the specified final concentrations: pectin (0.7% w/w), starch (5.15% w/w), sucrose (4.57% w/w), and then sodium chloride (0.534% w/w). During this process the samples were continually stirred to ensure each component was fully dissolved.

In some studies, the fluid form of the standardized food model was converted into a powder using spray drying. The fluid form was passed into a bench-top spray dryer (Mini Spray-dryer B-290, Büchi, Switzerland) at a feed rate of 0.45 L/h and inlet temperature of 170 °C and sprayed through a 0.7 mm nozzle atomizer. The obtained powders were then collected and stored in a hermetically sealed vessel at 4 °C until use.

To prepare 100g of the SFM, a weighed amount of the powder (17.8g) was slowly added into double distilled water (82.2g) that was continually stirred using a magnetic stirrer. It is suggested to stir at least 30 min at room temperature to ensure the powder is completely dispersed.

2.3. Determination of particle characterization of standardized food model

The particle size of the SFM was measured after sequentially adding each of the components using static light scattering (Mastersizer 2000, Malvern Instruments Ltd., Malvern, Worcestershire, UK). The electrical surface potential (ζ-potential) of the samples was determined using an electrophoresis instrument (Zetasizer Nano ZA series, Malvern Instruments Ltd. Worcestershire, UK). The refractive indices of the oil and water phases used in the calculations were 1.47 and 1.33, respectively. Samples were diluted with phosphate buffer (10 mM) of the appropriate pH to avoid multiple scattering effects. The particle size and surface potential were calculated automatically using the software associated with each instrument. All experiments were carried out in triplicate using freshly prepared samples. Means and standard deviations were calculated from a minimum of three measurements using Excel.

It should be noted that light scattering data should be treated cautiously for complex systems that contain multiple kinds of colloidal particles that can scatter light, since they all contribute to the measured signal. Moreover, the particle size distribution obtained may depend on the degree of dilution and stirring. Consequently, the results should only be used as a rough estimate of the actual particle size in these systems.

2.4. Microstructure analysis of standardized food model

The distribution of the emulsified oil in the samples was analyzed using confocal laser scanning microscopy (CLSM) with a 40 × objective lens (Nikon D-Eclipse C1 80i, Nikon, Melville, NY, U.S.). The oil phase was dyed using 0.10 mL of Nile red solution (1.00 mg mL^{-1} ethanol) to 2.00 mL of sample and the protein was dyed using fluorescein thiocyanate isomer I (FITC) solution (1.00 mg/mL dimethyl sulfoxide) by adding 0.10 mL of FITC dye solution to 2.00 mL of sample. The resulting confocal microstructure images were analyzed using image analysis software (NIS-Elements, Nikon, Melville, NY).

2.5. Colorimetry of standardized food model

The appearance of food powders depends on their composition and microstructure and so provides an indication of their performance and batch-to-batch variation. The tristimulus color coordinates of the samples were, therefore, measured using an instrumental colorimeter (ColorFlez EZ, HunterLab, Reston, Virginia, US): L^* (lightness); a^* (red to green); and, b^* (yellow to blue). The SFM samples were measured in the fluid state (i.e., after each adding each of the components) or in the powdered state (i.e., after spray drying). Two commercial food powders (i.e., baby formula and coffee creamer) were also measured in the powder state for comparison.

2.6. Gastrointestinal tract simulation studies

The properties of freshly produced SFM were determined using a simulated gastrointestinal model that included the mouth, stomach and small intestine phases. This model was adopted from our previous study with some modifications (DeLoid, et al., 2017b) and draws from earlier works on the *in vitro* digestion of food components, particles, and contaminants (Bohmert, et al., 2014; Versantvoort, Oomen, Van de Kamp, Rompelberg, & Sips, 2005). A brief summary is listed below.

Initial System: 20.0 g of SFM were preheated in an incubator shaker at a rotation speed of 100 rpm at 37 °C for 15 min (Innova Incubator Shaker, Model 4080, New Brunswick Scientific, Edison, NJ).

Mouth phase: Simulated saliva fluid (SSF) containing 0.0030 g/mL mucin and 150 units/mL amylase was pre-adjusted to pH 6.8 and then preheated to 37 °C. The initial samples were then mixed with an equal mass of SSF with continual stirring. After being re-adjusted to pH 6.8, the mixture was incubated in an incubator shaker (37 °C) for 2 min to mimic agitation in the mouth.

Stomach phase: 20.0 g of the samples resulting from the mouth phase was mixed with an equal mass of preheated (37 °C) simulated gastric fluid containing 0.0032 g/mL pepsin. The mixture was adjusted to pH 2.5 and then kept in the incubator shaker at 37 °C for 2 h to mimic stomach conditions.

Small intestine phase: 30.0 g of sample from the stomach phase was placed in a 100 mL glass beaker preheated in a water bath to 37 °C, and then the solution was adjusted to pH 7.00. 1.50 mL of simulated intestinal fluid (mixture of NaCl and $CaCl_2$) and 3.50 mL of bile salt solution were successively added to the reaction vessel with constant stirring. After the mixture was adjusted back to pH 7.00, 2.50 mL of pancreatin solution was added. The final concentration of NaCl, $CaCl_2$, bile salts and pancreatin in the reaction cell were: 150 mM, 10.0 mM, 5.0 mg/mL and 2.40 mg/mL, respectively. An automatic titration unit (Metrohm, USA Inc.) was used to keep the mixture at pH 7.0 by titrating 0.1 N NaOH solution into the reaction vessel for 2 h at 37 °C.

The particle characteristics and microstructure of the samples after each digestion stage (mouth, stomach and small intestine) were determined based on the methods described in previous sections.

2.6.1. Lipid Digestion—The amount of lipid that was digested during the small intestine phase was determined from the pH stat data. The volume of 0.1 N NaOH (mL) required to neutralize the free fatty acids (FFA) released during lipid digestion was recorded throughout the 2 h digestion period. The level of free fatty acids released was then calculated from these titration curves as previously described (Li & McClements, 2010). SFM samples were prepared without lipids so that the amount of free fatty acids released could be calculated by comparing the titration curves in the presence and absence of lipids.

2.6.2. Protein Digestion—The amount of protein that was digested (free α-amino groups) by the end of the small intestine phase was determined using the reaction agent *o*-phthaldialdehyde (OPA)(Nielsen, Petersen, & Dambmann, 2001; Yi, Van Boekel, Boeren, & Lakemond, 2016) and calculated using the following approach. An aliquot (10 to 30 μL) of sample was added to reagent (1 mL) and incubated for 2 min at room temperature after which the absorbance (340 nm) was measured (Schasteen, Wu, Schulz, & Parsons, 2007). The degree of hydrolysis (DH) was then calculated based on the following formula (Hardt, Van der Goot, & Boom, 2013; Nielsen, et al., 2001):

$$\mathrm{DH}(\%) = \frac{(\mathrm{Serine} - NH_2 - \beta)}{\alpha h_{tot}}$$

where

$$\mathrm{Serine}-NH_2 = \frac{A_{hydr} - A_{OPA}}{(X \times P)/L} \times \frac{mM\ serine}{A_{serine} - A_{OPA}}$$

Here, Serine-NH_2 is the meqv of serine-NH_2 per gram of protein, A_{hydr} is the absorbance of the casein hydrolysate sample, A_{OPA} is the absorbance of the blank OPA reagent, and Aserine is the absorbance of the serine standard. X is the weight (g) of sample and P is the concentration (%) of protein in the sample. The parameters h_{tot} is 8.2, α is 1.039 and β is 0.383 for casein. The calculated DH% was the mean of four determinations.

2.6.3. Starch Digestion—The amount of starch that was digested by the end of the small intestine phase was calculated as follows. After the final intestinal digestion, the digesta was centrifuged and the glucose concentration in the digesta was measured with a commercial glucose meter (Accu Check® Performa® glucometer, Roche). The amount of digested starch per 100 g dry starch (DS) was calculated using the following expression:

$$\mathrm{DS} = \frac{0.9 \times G_G \times 180 \times V}{W \times S}$$

Here, G_G = the glucometer reading (mM/L), V = the volume of digesta (mL), 180 = the molecular weight of glucose, W = the weight of sample (g), S = the starch content of sample (g per 100 g dry sample), and 0.9 = stoichiometric constant for starch from glucose contents (Sopade & Gidley, 2009).

2.7. Properties of powder form of standardized food model

The properties of the powdered form of SFM as prepared by spray drying were tested and compared to those of two commercial food powders (baby formula and coffee creamer). Once reconstituted in water, the colloidal properties of the powdered SFM were also tested against fresh batches of the SFM that had not been dried.

2.7.1 Hydration properties—The water solubility index (WSI) of the SFM powders was determined based on an AACC method (No. 44–19) with some slight modifications(Aacc, 2000). Specifically, the powder (S1, g) was weighed into a centrifuge tube and then water was added at a powder-to-water ratio of 0.020 (w/w). The resulting dispersion was then incubated in a water bath at room temperature for different times (30–240 min) or at different temperatures (25–80 °C) for a fixed time (30 min), followed by centrifugation at 6000 rpm for 5 min. The supernatant was collected in a pre-weighed evaporating dish (S2, g) and then dried at 103 ± 2 °C, and the evaporating dish with residue was weighed again (S3, g). The WSI was calculated using the following formula: WSI (%) = (S3−S2)/S1*100%.

2.7.2 Flow properties determination—The flowability of the SFM powders was determined by measuring the angle of repose, slide angle, and bulk density. The angle of repose was measured according to the method reported by Zhang et al. (2012)(Zhang, et al., 2012). Firstly, a funnel was fixed vertically above a piece of graph paper with a fixed distance (H) from the paper to the outlet of the filler. Then, the powder was continuously poured into the funnel and went out freely until the tip of the powder cone reached the outlet of the funnel. The diameter (2R) of the cone was determined based on the marked scale on the paper and then the angle of repose (h) was calculated as the following formula: h = arctan H/R.

The slide angle (α) was determined according to the procedure described by Zhou and Ileleji(Ileleji & Zhou, 2008) with some slight modifications. Specifically, 0.3 g of test powder was weighed and then poured on a rectangular glass plane with a length of 11 cm. The glass plane was then gradually lifted until the surface of the test powders began to slide. The vertical distance (H) from the top of the inclined glass plane to the horizontal was recorded and the angle of slide (α) was calculated using the following formula: α = arcsin H/L.

The bulk density was measured by gently pouring 0.3 g of test powders into a 10 mL measuring cylinder, and then holding the cylinder on a vortex vibrator until a constant volume of the sample was obtained. The sample volume was then recorded against the scale on the cylinder. The bulk density was then calculated as the ratio of the mass of the powder and the volume occupied in the cylinder(Bai & Li, 2006).

2.7.3 Moisture sorption isotherms—The moisture sorption isotherm of the powders was determined according to a previously described method with some slight modifications (Lee & Lee, 2007). The equilibrium moisture content of the test powders was determined gravimetrically using the Conway dish method. Eight different saturated salt solutions, including NaOH, $MgCl_2$, $Mg(NO_3)_2$, NaCl, KBr, KCl, BaCl and $K_2Cr_2O_7$, were poured in the outer layer of the Conway dish to obtain a range of water activities from 0.07 to 0.986. The moisture sorption value was then determined by placing 0.3 g of test powder in a weighed bottle and then put inside the inner layer of the Conway dish, which was firmly sealed and stored at room temperature. All the test samples were weighed every 24 h until equilibrium was achieved, *i.e.,* two consecutive weights less than ± 0.0005 g. The moisture content of the powder samples was then determined by drying them in an oven at 105 °C for 12 h (AACC method of No. 44–19). The GAB isotherm models (Guggenheim-Anderson-de Boer) was used to fit the experimental moisture sorption date as follows:

$$X = X_0 CK a_W / \left[(1 - K a_W)(1 - K a_W + C K a_W) \right] \quad (1)$$

Here, X is the moisture content, X_0 is the monolayer moisture content, a_w is the water activity, C is a constant related to molecular interactions of the water molecules in the monolayer of adsorbed water with the powder, and K is a constant related to the molecular interactions of the water in the multilayer of adsorbed water with the powder.

2.8. Nanotoxicology case study: Assessment of toxicity of ingested TiO_2 using an *in vitro* cellular model of gut epithelium

2.8.1. Characterization of TiO_2—Food grade TiO_2 particles (E171) were purchased from an online retailer. A thorough physical and chemical of their properties has been reported elsewhere (Lee, et al., 2018). Briefly, the primary particles had a mean diameter of around 113 nm as determined by TEM and were in the anatase form.

2.8.2. Suspension of ENMs—Titanium dioxide (TiO_2) ENMs (E171) were suspended in 5 mM phosphate buffer (fasting medium) and in reconstituted standardized food model (SFM) at 0.75% w/w and 1.5% w/w. Before adding E171 particles to either the fasting medium or SFM, they were first vortexed and then sonicated for 30 and 10 seconds, respectively. This step was performed to create the smallest possible agglomerates of E171 and was achieved by following a standardized method described previously (Cohen, Beltran-Huarac, Pyrgiotakis, & Demokritou, 2018; DeLoid, Cohen, Pyrgiotakis, & Demokritou, 2017a).

2.8.3. Suspension and GIT simulated digestion of ENMs—The simulated digestion of the TiO_2 nanoparticle suspension in food media was performed using a benchtop, three-stage gastrointestinal tract (GIT) simulator of the mouth, stomach and small intestinal phases as described earlier. Briefly, for the mouth phase, TiO_2 nanoparticles were suspended in either fasting medium or SFM, mixed, and then incubated for 2 min with simulated saliva fluid composed of different salts and porcine gastric mucin type II. The resultant mouth digestae ("bolus") were then mixed and incubated for 2 h with a simulated gastric fluid composed of sodium chloride and hydrochloric acid to represent the stomach digestion phase. In the small intestinal phase, the stomach digestae ("chyme") were mixed with bile salts and proteins to simulate the intestinal fluids. This system was then incubated for 2 h at a constant pH of 7.0 using a pH Stat device. At the end of digestion, samples were collected and mixed with serum-free cell culture media at a ratio of 1:3 (vol:vol) before adding them to the cell culture.

2.8.4. Tri-cellular in vitro culture model of the gut epithelium—To prepare the *in vitro* tri-cellular culture (triculture) gut epithelium model, the protocol described by Deloid et al. (DeLoid, et al., 2017c) was followed. Briefly, cryopreserved Caco-2, HT29-MTX, and Raji B cells tested and confirmed at the European Collection of Authenticated Cell Cultures (ECACC), were purchased from Sigma-Aldrich. The cells were thawed by immersion in a water bath (37°C), diluted in 10 ml of growth medium, and subsequently centrifuged at 100 × g. The supernatant was carefully aspirated, and the pellet was resuspended with the addition of fresh growth medium. At the time of the experiments, the passage numbers for Raji-B, Caco-2, and HT29-MTX cell cultures were respectively 7, 49, and 51. Caco-2 and HT29-MTX cells were grown in high-glucose DMEM cell culture medium supplemented with 10% heat-inactivated fetal bovine serum (FBS), 10 mM HEPES buffer, 100 IU/ml Penicillin, 100 μg/ml Streptomycin, and non-essential amino acids (1/100 dilution of 100 X solution, ThermoFisher). Raji B cells were cultured in RPMI 1640 cell culture medium supplemented with 10% FBS, 10 mM HEPES buffer, 100 IU/ml Penicillin, and 100 μg/ml Streptomycin.

The Caco-2 and HT29-MTX cells were trypsinized using 5 mL TrypLE™ and detached from the bottom of the flask; 10 mL of complete DMEM media were then added to the flasks and mixed with the detached cells. The resuspended cells were then centrifuged at 100xg to pellet the cells; the pellet was then resuspended in fresh, complete DMEM media at a concentration of 3×10^5 cells/cm^3. The Caco-2 and HT29-MTX cells were combined at a ratio of 3:1. 1.5 ml of the cell mixture was seeded in the apical chamber of the transwell plate (Sigma-Aldrich, US) and 2.5 ml of complete DMEM media was added to the basolateral compartment of a 6-well transwell plate. The first change of media for the cells in transwells was done four days after seeding, and repeated every other day until the plates were 10 days old. From culture days 10 to 15, the medium was changed every day. On the fifteenth day, the medium in the basolateral compartment was substituted by a 2.5ml Raji B cell suspension at a concentration of 1 million cells/ml in 1:1 DMEM:RPMI complete medium. This procedure was repeated for a second day of Raji B cell treatment, completing a total of seventeen days of culture for the transwell plates, at which point they were ready to be used for toxicity or biokinetics experiments (Deloid et al., 2017).

2.8.5. Cytotoxicity analysis: Digestae of TiO_2 mixed were mixed with fasting medium or SFM at starting concentrations of 0.75% and 1.5% w/w and then passed through the simulated GIT described above. The resulting digestae were then mixed with serum-free RPMI-1640 :DMEM (1:1) media in the ratio of 3:1. The TiO_2 digestae and cell culture mixture were added to the GIT tri-culture model and the cells were incubated for 24 hrs. At the end of the exposure period, samples of the cell culture media were collected from the apical and basolateral compartments of the GIT tri-culture, mixed, and stored at −80°C until further analysis. For measuring cytotoxicity, a lactate dehydrogenase (LDH) release assay was performed. Using the Pierce LDH cytotoxicity assay kit (Themofischer Scientific, IL) and the associated protocol absorbance were measured at wavelengths of 490 and 680 nm, and then the cytotoxicity percentage was calculated.

2.9. Statistical analyses

All experiments were performed on at least three freshly prepared samples. The results are reported as averages and standard deviations. These analyses were carried out using Excel (Microsoft, Redmond, VA, USA) and a statistical software package (SPSS). All nanotoxicology experiments were performed thrice in duplicates and the statistical significance of the results was tested using One-way ANOVA with Bonferroni *post-hoc* test using SigmaPlot® v11 software.

3. Results and Discussion

3.1. Standard food model preparation and characterization

The overall aim of this study was to fabricate a *standardized meal* that could be used to study the impact of food matrix effects on the gastrointestinal fate and potential toxicity of ingested NPs. The SFM was designed to have a number of attributes that would facilitate its widespread application: (i) ease of fabrication; (ii) good stability; (iii) small initial particle size; and (iv) narrow and reproducible particle size distribution. Preliminary experiments were carried out to determine the impact of adding the various dietary components (protein,

fat, sugar, starch, dietary fiber, and minerals) to the initial emulsion in different orders. It was determined that order-of-addition did have a pronounced impact on the stability and properties of the final product. For instance, there were differences in the tendency for the various components in the final systems to aggregate and separate depending on when they were added, which was primarily attributed to differences in the nature of the colloidal interactions and rheological characteristics in the system throughout the preparation procedure. The optimum preparation procedure was therefore defined as the order-of-addition sequence that led to good stability, small particle size, and narrow particle size distribution. This procedure involved adding the different components to the casein-stabilized emulsions in the following order and final concentrations: pectin (0.70%), starch (5.15%), sucrose (4.57%) and sodium chloride (0.534%).

The mean particle diameter, surface potential, viscosity, color, and microstructure of SFM were measured at each stage during its fabrication using the optimized method. There was little change in the particle size distribution (Figure 1a) and mean particle diameter (Figure 1b) of SFM after the addition of each food component, which suggests that the systems were relatively stable to aggregation. However, it should be noted that the samples had to be diluted (at least four-fold) prior to analysis by the laser diffraction instrument so as to avoid multiple scattering effects, which may impact the particle size (see later). The good aggregation stability of the samples can be attributed to the fact that both the casein-coated oil droplets and the pectin molecules in SFM were negatively charged at pH 7 (Surh, Decker, & McClements, 2006), and so there would be a strong electrostatic repulsion between them. The presence of the other components in the SFM (starch, sucrose, and sodium chloride) did not have a major impact on the particle size (Figures 1a and 1b). The starch and sucrose are both neutral molecules and would not therefore be expected to impact the electrostatic interactions in the system. The level of NaCl added was fairly low (91 mM) and so therefore only be expected to have a minor influence on the electrostatic interactions. The ζ-potential on the particles in SFM became slightly less negative when pectin was added to the casein-coated emulsions but did not change much when the other ingredients were added (Figure 1c). The reduction in the magnitude of the negative charge in the presence of pectin may have been because it contributes to the electrophoretic mobility signal used to calculate the ζ-potential or because some of it adsorbed to the protein-coated droplet surfaces. There was a slight decrease in ζ-potential after the NaCl was added to the system, which is probably due to electrostatic screening effects.

The light scattering experiments suggested that there was no aggregation of the particles in SFM after adding the different food components (Figure 1), however, the confocal microscopy results suggested otherwise. The microscopy images indicated that there was pronounced aggregation of the oil droplets after pectin addition and then some further changes in the aggregation state of the system after addition of the other food components (Figure 2). This result can be attributed to the flocculation of the oil droplets in the presence of pectin. It has previously been reported that non-adsorbed pectin can promote depletion flocculation in oil-in-water emulsions when it exceeds a certain level due to an osmotic exclusion effect (Guzey & McClements, 2006). The pectin molecules are excluded from a narrow region surrounding each oil droplet and so their effective concentration in this “exclusion zone” is zero. Consequently, there is an imbalance in pectin concentration

between the exclusion zone and the surrounding aqueous phase, which generates an osmotic stress. The magnitude of this osmotic stress increases as the concentration of pectin in the system increases. At a sufficiently high pectin concentration, the magnitude of the osmotic stress becomes larger than the repulsive forces acting between the droplets and promotes flocculation. When the emulsions are diluted for laser diffraction analysis, the pectin concentration is reduced thereby decreasing the osmotic stress, causing the flocs to dissociate. This phenomenon therefore accounts for the fact that flocculation was observed in the confocal microscopy images (Figure 2), but not in the particle size data obtained by laser diffraction (Figure 1). The addition of starch, sugar, and NaCl caused some changes in the nature of the flocs formed but the oil droplets were still aggregated. Importantly, in all cases, the flocs could be disrupted when they were diluted for particle size analysis, which may be important when studying the impact of food matrix effects on the gastrointestinal fate of inorganic nanoparticles.

The stability of SFM to gravitational separation was established by monitoring changes in their appearance during storage. Our results showed that they were stable to creaming throughout two days' incubation at ambient temperature, even though flocs were still visible in the confocal microscopy images (data not shown). The lack of creaming in the freshly prepared samples can be attributed to two physical phenomena that inhibit droplet movement: (i) an increase in the viscosity of the aqueous phase surrounding the droplets; (ii) the formation of a three-dimensional network of flocculated oil droplets (Chung, Degner, & McClements, 2014). For this reason, the rheological properties of SFM were measured after the addition of each food ingredient. The viscosity of the initial emulsions was low (1.7 mPa s) but they contained small oil droplets (d = 127 nm) that were not flocculated, which would account for their good creaming stability. All the other emulsions had relatively high viscosities, which would have slowed down the movement of the oil droplets in the system. Pectin and starch are relatively large hydrophilic molecules that increase the viscosity due to their ability to interfere with fluid flow. On the other hand, the presence of sugar and salt in the aqueous phase may have altered the molecular and colloidal interactions in the system. For instance, salt screens electrostatic interactions, whereas sugars increase osmotic effects.

The optical properties of emulsions can provide valuable insights into their stability, since their appearance depends on droplet concentration, size, and aggregation state (McClements, 2002). The optical properties of SFM were therefore measured using an instrumental colorimeter after each food component was added (Figure 4). The lightness (L* value) of the casein-stabilized emulsions did not change appreciably after the addition of pectin, starch, or sugar suggesting that there was not a large change in emulsion properties (Figure 4). However, there was an appreciable increase in the lightness of SFM after addition of sodium chloride, suggesting that more light scattering occurred. This result may be attributed to a change in the structural organization of the oil droplets in SFM after salt addition, as seen in the confocal fluorescence microscopy images (Figure 2). Presumably, the scattering efficiency of the oil droplets was increased because of this structural change so that the light beam was reflected more efficiently from the surface of SFM. Having said this, the overall change in the L* value was only relatively small (around 2 units).

3.2. Standard food model powder properties

To facilitate the practical application of the SFM it was converted into a powdered form using spray drying. Compared to the fluid form, the powdered form has a longer shelf life, requires less storage space, does not need refrigeration, and should be easier to use. The physical properties of the powdered SFM were measured and compared to those of original wet SFM, as well as to those of two commercial food powders: baby formula and coffee creamer. These comparisons were made because commercial food powders are formulated to have long shelf-lives, high flowability, and good water-dispersibility, which are all important characteristics for a SFM that might be used widely by many researchers.

The *water solubility index* (WSI) of the powdered SFM increased appreciably when it was rehydrated at higher temperatures, with an approximately linear increase in WSI with increasing temperature (Figure 5a). There was also an increase in the water solubility index with increasing dispersion time at ambient temperature (Figure 5b). These results suggest that using higher temperatures or longer incubation times will lead to quicker dispersion of the fat droplets and other components in the powders. The *repose angle* provides a rough indication of powder flowability: angles lower than 35° indicate free flowability, 35° - 45° partial cohesiveness, 45° - 55° cohesiveness (loss of free flowability), and 55° and above very high cohesiveness and very limited flowability (Chang, Kim, Kim, & Jung, 1998). Based on this classification, SFM and coffee creamer showed free flowability while the baby formula exhibited partial cohesiveness (Table 2). This trend was also seen in the *slide angle* measurements: the baby formula had a much higher slide angle than SFM and coffee mate, indicating much lower flowability. This result might be due to the higher protein content of the baby formula powders. Previous studies have shown that powder cohesiveness increases as their protein content increases (Chang, et al., 1998). The bulk density measurements showed that the powdered SFM had a higher density that the two commercial powders (Table 2). This effect might be due to the fact that commercial food powders often undergo an agglomeration step after spray drying to facilitate their subsequent rehydration, but this step was not carried out for SFM. Agglomeration leads to more pore spaces between powder particles thereby decreasing the bulk density (Zhao, Ao, Du, Zhu, & Liu, 2010).

The optical properties of food powders provide valuable insights into their properties, such as physical state and chemical stability. For this reason, the tristimulus color coordinates of the powders were measured using an instrumental colorimeter. The color measurements showed that SFM powders had relatively high L^* values compared to the two commercial powders (Table 2). The lower L^* values in the commercial products may have been a result of agglomeration (an increase in particle size) or browning reactions (such as Maillard reactions). The a^* values of all the powders were close to zero, indicating that they had little green-red color. All the b^* values of the powders were positive, suggesting that they had a yellowish color. However, there were appreciable differences between the magnitude of the b^* values, with the intensity of the yellow color being much less in SFM powder than in the baby formula. Again, this may be due to differences in the particle size or chemical composition of the powders. The differences in the optical properties of the powders could also be observed in their visual appearances (Figure 6). Overall, these results suggest that SFM forms a powder that has a strongly whitish appearance.

The tendency for a powder to adsorb water from its environment under different relative humidity conditions can be described by its moisture sorption isotherm. For this reason, the equilibrium moisture content (EMC) of the different powders was measured against the water activity (a_w) of the environment at 25 °C (Figure 7). The moisture sorption isotherms showed an increase in equilibrium moisture content with increasing water activity with a sigmoid shape for all three test powders. This result indicated that all three powders exhibited Type III behavior according to Brunauer's classification, *i.e.,* the powders behaved like amorphous materials rich in hydrophilic components (Rizvi, 1995). As the water activity increases, the water molecules first bind to the surfaces of the molecules in the powder as monolayers (low moisture regime) then multilayers (intermediate moisture regime), but then they form a separate bulk phase around the dissolved molecules (high moisture regime) (Goula, Karapantsios, Achilias, & Adamopoulos, 2008). The three test powders showed slightly different moisture sorption isotherms, which can mainly be attributed to differences in their composition *e.g.,* sugar, starch, protein, and salt content. The moisture sorption isotherms of the different powders were fitted using the GAB model (Figure 7). There was good agreement between the measured and predicted isotherms across the entire a_w range for all the samples. The fitted parameters used in the GAB model and correlation coefficients are given in Table 2. The K and C values provide a measure of the interactions between the water molecules and the molecules in the powders. The X_0 value is related to the monolayer moisture content, which indicates the amount of water strongly adsorbed to specific sites on the molecules in the powder (Gabas, Telis, Sobral, & Telis-Romero, 2007). Overall, these results indicate that the powdered SFM has physicochemical characteristics fairly similar to those of commercial food powders, which should facilitate its practical application.

The reconstituted SFM properties (particle size, surface charge, microstructure) were also measured. There was no significant difference observed compared with the fresh samples (data was not shown), which indicated that spray drying followed by reconstitution leads to a product similar to the fresh one.

3.3. Digestion properties of SFM and the effects of spray-drying

In this section, we determined the potential gastrointestinal fate of SFM using an *in vitro* digestion model that simulates the conditions in the mouth, stomach, and small intestine. The characteristics of the freshly produced (fluid) SFM and a batch that was reconstituted after it was spray-dried were compared to determine whether dehydration and reconstitution causes any undesirable effects on its GIT behavior. An automatic titration (pH stat) method was used to evaluate the digestion of SFM in the small intestine phase. Porcine pancreatin was selected as the source of digestive enzymes for the intestinal phase because it contains all the important pancreatic enzymes (lipases, proteases, amylases) required to digest the major components in SFM (fats, proteins, and starches) (Minekus, et al., 2014).

The volume of NaOH (0.1 N) solution titrated into the samples to maintain a constant pH (7.0) was measured as a function of digestion time in the small intestine stage (Figure 8). These results indicated that the digestion profiles of SFM were similar for both the fresh and the reconstituted form. In both cases, there was a rapid increase in NaOH added during the

first 10 minutes of digestion, followed by only a gradual increase at longer incubation times. This result suggests that the majority of SFM had been digested by the end of the small intestine phase. The degree of starch and protein hydrolysis by the end of the small intestine phase were around 54.9% and 67.9%, respectively. These values are in good agreement with previous studies, and suggest that most of the starch had been converted to sugars and oligosaccharides and most of the protein had been converted to amino acids and peptides(Alonso, Aguirre, & Marzo, 2000; Sopade, et al., 2009).

The particle size and electrical characteristics of the particles in the fresh and reconstituted samples were measured as they passed through the various stages of the simulated GIT (Figure 9). It should be noted that the samples contain a variety of different colloidal particles and polymers that could contribute to the signals used to determine particle size and charge, and so the results reflect the net effect. As discussed in the previous section, the relatively high negative charge on the particles in the initial samples (−37.8 and −31.9 mV) can be attributed to the presence of anionic casein-coated droplets and anionic pectin molecules in SFM at pH 7. After incubation in the simulated mouth conditions, there was a slight decrease in the magnitude of the negative charge for both the fresh (−35.3 mV) and reconstituted (−31.2 mV) SFM. These slight changes might be due to the presence of mineral ions and mucin in the simulated saliva, which reduced the magnitude of the ζ-potential through ion binding or electrostatic screening effects. There was a further decrease in the magnitude of the negative charge (−1.8 mV and −3.1 mV) on both samples after passing through the stomach phase. This effect is due to a number of reasons. First, the casein-coated oil droplets become positively charged under highly acidic conditions because the pH is well below their isoelectric point (around pH 4.6). Second, the pectin molecules lose most of their negative charge under highly acidic conditions because the majority of their carboxyl groups (pKa = 3.5) become protonated (-COOH). Furthermore, anionic mucin and pectin molecules may have adsorbed to the surfaces of the cationic casein-coated droplets under gastric conditions, leading to a slight negative charge on the particles in the stomach phase (Gabas, et al., 2007). After incubation in the small intestinal phase, both samples again showed relatively high negative charges. This can be attributed to the fact that various kinds of anionic particles are present in the neutral pH conditions present in the small intestine phase after lipid digestion, including mixed micelles, calcium salts, partially digested lipids, and pectin molecules(Zhang, Zhang, Zhang, Decker, & McClements, 2015).

The particle size distributions of both fresh and reconstituted SFM determined by laser diffraction exhibited a single peak representative of a population of relatively small particles in the initial samples and after exposure to the mouth phase (Figure 9). However, the confocal microscopy images indicated that there was some flocculation in these systems (Figure 10). Again, this effect suggests that the oil droplets were present in flocs that were held together by relatively weak interactions that dissociated when the samples were diluted for the laser diffraction measurements. After exposure to the simulated gastric conditions, both the laser diffraction and confocal microscopy measurements indicated that the droplets in both samples became highly aggregated, suggesting that strong flocculation or coalescence occurred. This effect may have occurred for a number of reasons: (i) pepsin in the stomach phase hydrolyzed the casein adsorbed to the fat droplet surfaces, thereby promoting droplet flocculation and coalescence; (ii) the low ζ-potential of the oil droplets

and high ionic strength of the gastric fluids weakened the electrostatic repulsion thereby promoting droplet aggregation. After the small intestine phase, there was evidence of a few lipid-rich particles in the confocal microscopy images (Figure 10), which may have been lipid digestion products (such as vesicles or calcium soaps) or a small amount of residual undigested fat (Zhang, Zhang, Zou, & McClements, 2016). These relatively large particles were also detected by laser diffraction (Figure 9).

3.4. Cytotoxicity assessment of TiO_2 using the standardized food model

The recorded levels of lactate dehydrogenase (LDH) showed that food-grade TiO_2 nanoparticles dispersed in fasting medium compromised the cellular membranes of the modelled gut epithelium (Figure 11). The digestae of fasting medium with the highest concentration of TiO_2 particles exhibited the strongest cytotoxicity ($p < 0.001$). Interestingly, the TiO_2 in the standard food model digestae were less cytotoxic against the same triculture model when compared to their fasting medium counterparts. This reduction in cytotoxicity as a result of the food matrix effect was found to be statistically significant ($p = 0.01$) at both concentrations (0.75% and 1.5% w/w) when compared with the same amount of particles in the fasting medium. For the 1.5% w/w system, the decrease in toxicity was around 5-fold in the presence of the SFM (Figure 11). The precise origin of this effect is currently unknown and certainly warrants further studies. It does, however, highlight the importance of food matrix effects when studying their toxicity against the gut epithelium. In our case, it is possible that the TiO_2 nanoparticles interacted with some of the constituents in the standardized food model, which changed their surface characteristics and/or aggregation state, thereby altering their ability to move through the mucus layer and be absorbed by the model epithelium cells.

Overall, we contend that combining the standardized food model with a standardized GIT model will provide a more realistic assessment of the impact of food matrix effects on the toxicological assessment of ENMs. In particular, it provides a useful tool in the field of nanotoxicology for screening changes in the particles' biokinetics and potential toxicity. At the same time, we acknowledge that there are no *in vitro* models that can perfectly mimic the mechanical, chemical, and biochemical conditions in the human digestive tract. Therefore, animal studies should be the next step for an in-depth assessment of the pathogenicity of ingested ENMs.

4. Conclusion

In this study, we developed a food model based on the reported nutrient composition of the US diet. This model contained representative proteins, fats, dietary fibers, and carbohydrates at levels typically found in the human diet. Structurally, SFM consisted of an oil-in-water emulsion containing protein-coated fat droplets dispersed in an aqueous solution contain free protein, starch, pectin, sugar and salt. The physical measurements indicated that there was little change in the particle size and charge of the individual oil droplets, but an increase in apparent viscosity of the SFM after each food component was added. The fluid SFM could be converted into a powdered form by spray drying so as to increase its shelf life and facilitate its practical application. The physical properties of the powdered SFM, such as

hydration, flowability, and moisture sorption, were fairly similar to those of commercial food powders indicating that it should be suitable for widespread utilization. SFM was passed through a commonly used simulated gastrointestinal model and changes in its structural properties were characterized. The main food components in the SFM were shown to be digested when exposed to the digestive enzymes in the simulated GIT. Finally, we showed that the potential toxicity of the titanium dioxide nanoparticles was reduced in the presence of the SFM, which highlighted the importance of food matrix effects.

This information should be useful when designing experiments to test food matrix effects on the toxicity of inorganic nanoparticles. In particular, the availability of a standardized food model will facilitate the comparison of results obtained on food matrix effects from different laboratories. In this study, we developed a standard food model to represent the typical American diet. In future studies, we intend to develop additional food models for other more specialized diets, including high-fat, high-sugar, or high-protein diets.

Acknowledgements

This material was partly based upon work supported by the Cooperative State Research, Extension, Education Service, USDA, Massachusetts Agricultural Experiment Station (MAS00491) and USDA, NRI Grants (2013–03795). Research reported in this publication was supported by the HSPH Center for Nanotechnology and Nanotoxicology and National Institute of Environmental Health Sciences of the National Institutes of Health (under award number, NIH grant # U24ES026946) as part of the Nanotechnology Health Implications Research (NHIR) Consortium. The content is solely the responsibility of the authors and does not necessarily represent the official views of the National Institutes of Health.

6. References

Aacc I. (2000). Approved Methods of the AACC. Association of Cereal Chemists, St. Paul

Ahluwalia A, Boraschi D, Byrne HJ, Fadeel B, Gehr P, Gutleb AC, Kendall M, Papadopoulos M, & Lynch I (2013). The bio-nano interface as a basis for predicting nanoparticle fate and behavior in living organisms: towards grouping and catergorizing of nanomaterials and nanosafety by design. Bio Nano Materials, 14, 195–216.

Alonso R, Aguirre A, & Marzo F (2000). Effects of extrusion and traditional processing methods on antinutrients and in vitro digestibility of protein and starch in faba and kidney beans. Food chemistry, 68(2), 159–165.

Bai Y-X, & Li Y-F (2006). Preparation and characterization of crosslinked porous cellulose beads. Carbohydrate polymers, 64(3), 402–407.

Bohmert L, Girod M, Hansen U, Maul R, Knappe P, Niemann B, Weidner SM, Thunemann AF, & Lampen A (2014). Analytically monitored digestion of silver nanoparticles and their toxicity on human intestinal cells. Nanotoxicology, 8(6), 631–642. [PubMed: 23763544]

Bouwmeester H, van der Zande M, & Jepson MA (2018). Effects of food-borne nanomaterials on gastrointestinal tissues and microbiota. Wiley Interdisciplinary Reviews-Nanomedicine and Nanobiotechnology, 10(1).

Cao Y, Li J, Liu F, Li X, Jiang Q, Cheng S, & Gu Y (2016). Consideration of interaction between nanoparticles and food components for the safety assessment of nanoparticles following oral exposure: a review. Environmental toxicology and pharmacology, 46, 206–210. [PubMed: 27497726]

Chang KS, Kim DW, Kim SS, & Jung MY (1998). Bulk flow properties of model food powder at different water activity. International Journal of Food Properties, 1(1), 45–55.

Chung C, Degner B, & McClements DJ (2014). Development of reduced-calorie foods: microparticulated whey proteins as fat mimetics in semi-solid food emulsions. Food research international, 56, 136–145.

Cohen JM, Beltran-Huarac J, Pyrgiotakis G, & Demokritou P (2018). Effective delivery of sonication energy to fast settling and agglomerating nanomaterial suspensions for cellular studies: Implications for stability, particle kinetics, dosimetry and toxicity. NanoImpact, 10, 81–86. [PubMed: 29479575]

DeLoid GM, Cohen JM, Pyrgiotakis G, & Demokritou P (2017a). Preparation, characterization, and in vitro dosimetry of dispersed, engineered nanomaterials. Nature Protocols, 12(2), 355–371. [PubMed: 28102836]

DeLoid GM, Sohal IS, Lorente LR, Molina RM, Pyrgiotakis G, Stevanovic A, Zhang R, McClements DJ, Geitner NK, & Bousfield DW (2018). Reducing Intestinal Digestion and Absorption of Fat Using a Nature-Derived Biopolymer: Interference of Triglyceride Hydrolysis by Nanocellulose. ACS nano.

DeLoid GM, Wang Y, Kapronezai K, Lorente LR, Zhang R, Pyrgiotakis G, Konduru NV, Ericsson M, White JC, & De La Torre-Roche R (2017b). An integrated methodology for assessing the impact of food matrix and gastrointestinal effects on the biokinetics and cellular toxicity of ingested engineered nanomaterials. Particle and fibre toxicology, 14(1), 40. [PubMed: 29029643]

DeLoid GM, Wang Y, Kapronezai K, Lorente LR, Zhang R, Pyrgiotakis G, Konduru NV, Ericsson M, White JC, De La Torre-Roche R, Xiao H, McClements DJ, & Demokritou P (2017c). An integrated methodology for assessing the impact of food matrix and gastrointestinal effects on the biokinetics and cellular toxicity of ingested engineered nanomaterials. Particle and fibre toxicology, 14(1), 1–17. [PubMed: 28069023]

Eleftheriadou M, Pyrgiotakis G, & Demokritou P (2017). Nanotechnology to the rescue: using nano-enabled approaches in microbiological food safety and quality. Current opinion in biotechnology, 44, 87–93. [PubMed: 27992831]

Gabas AL, Telis VRN, Sobral PJA, & Telis-Romero J (2007). Effect of maltodextrin and arabic gum in water vapor sorption thermodynamic properties of vacuum dried pineapple pulp powder. Journal of Food Engineering, 82(2), 246–252.

Gao X, & Lowry GV (2017). Progress towards standardized and validated characterizations for measuring physicochemical properties of manufactured nanomaterials relevant to nano health and safety risks. NanoImpact.

Georgantzopoulou A (2015). Effects of silver nanoparticles and ions and interactions with first line of defense: Wageningen University.

Goula AM, Karapantsios TD, Achilias DS, & Adamopoulos KG (2008). Water sorption isotherms and glass transition temperature of spray dried tomato pulp. Journal of Food Engineering, 85(1), 73–83.

Guzey D, & McClements DJ (2006). Formation, stability and properties of multilayer emulsions for application in the food industry. Advances in colloid and interface science, 128, 227–248. [PubMed: 17223060]

Hardt NA, Van der Goot AJ, & Boom RM (2013). Influence of high solid concentrations on enzymatic wheat gluten hydrolysis and resulting functional properties. Journal of cereal science, 57(3), 531–536.

Ileleji KE, & Zhou B (2008). The angle of repose of bulk corn stover particles. Powder Technology, 187(2), 110–118.

Jain A, Ranjan S, Dasgupta N, & Ramalingam C (2018). Nanomaterials in food and agriculture: An overview on their safety concerns and regulatory issues. Critical reviews in food science and nutrition, 58(2), 297–317. [PubMed: 27052385]

Kaphle A, Navya PN, Umapathi A, & Daima HK (2018). Nanomaterials for agriculture, food and environment: applications, toxicity and regulation. Environmental Chemistry Letters, 16(1), 43–58.

Lee JY, Wang H, Pyrgiotakis G, DeLoid GM, Zhang Z, Beltran-Huarac J, Demokritou P, & Zhong W (2018). Analysis of lipid adsorption on nanoparticles by nanoflow liquid chromatography-tandem mass spectrometry. Anal Bioanal Chem.

Lee MJ, & Lee JH (2007). Moisture Sorption Isotherm Characteristics of Chaga Mushroom Powder as Influenced by Particle Size. Food Sci. Biotechnol, 16(1), 154–158.

Li Y, & McClements DJ (2010). New Mathematical Model for Interpreting pH-Stat Digestion Profiles: Impact of Lipid Droplet Characteristics on in Vitro Digestibility. Journal of agricultural and food chemistry, 58(13), 8085–8092. [PubMed: 20557040]

Lichtenstein D, Ebmeyer J, Knappe P, Juling S, Böhmert L, Selve S, Niemann B, Braeuning A, Thünemann AF, & Lampen A (2015). Impact of food components during in vitro digestion of silver nanoparticles on cellular uptake and cytotoxicity in intestinal cells. Biological chemistry, 396(11), 1255–1264. [PubMed: 26040006]

Lu X, Miousse IR, Pirela SV, Moore JK, Melnyk S, Koturbash I, & Demokritou P (2016). In vivo epigenetic effects induced by engineered nanomaterials: A case study of copper oxide and laser printer-emitted engineered nanoparticles. Nanotoxicology, 10(5), 629–639. [PubMed: 26559097]

McClements DJ (2002). Theoretical prediction of emulsion color. Advances in colloid and interface science, 97(1–3), 63–89. [PubMed: 12027025]

McClements DJ, DeLoid G, Pyrgiotakis G, Shatkin JA, Xiao H, & Demokritou P (2016). The role of the food matrix and gastrointestinal tract in the assessment of biological properties of ingested engineered nanomaterials (iENMs): State of the science and knowledge gaps. NanoImpact, 3, 47–57. [PubMed: 29568810]

McClements DJ, & Xiao H (2017). Is nano safe in foods? Establishing the factors impacting the gastrointestinal fate and toxicity of organic and inorganic food-grade nanoparticles. npj Science of Food, 1(1), 6.

Minekus M, Alminger M, Alvito P, Ballance S, Bohn T, Bourlieu C, Carriere F, Boutrou R, Corredig M, & Dupont D (2014). A standardised static in vitro digestion method suitable for food–an international consensus. Food & function, 5(6), 1113–1124. [PubMed: 24803111]

Mura S, Seddaiu G, Bacchini F, Roggero PP, & Greppi GF (2013). Advances of nanotechnology in agro-environmental studies. Italian Journal of Agronomy, 8(3), 18.

Nielsen PM, Petersen D, & Dambmann C (2001). Improved method for determining food protein degree of hydrolysis. Journal of food science, 66(5), 642–646.

Peters RJ, Bouwmeester H, Gottardo S, Amenta V, Arena M, Brandhoff P, Marvin HJ, Mech A, Moniz FB, & Pesudo LQ (2016). Nanomaterials for products and application in agriculture, feed and food. Trends in Food Science & Technology, 54, 155–164.

Pirela SV, Lu X, Miousse I, Sisler JD, Qian Y, Guo N, Koturbash I, Castranova V, Thomas T, Godleski J, & Demokritou P (2016). Effects of intratracheally instilled laser printer-emitted engineered nanoparticles in a mouse model: A case study of toxicological implications from nanomaterials released during consumer use. NanoImpact, 1, 1–8. [PubMed: 26989787]

Pirela SV, Pyrgiotakis G, Bello D, Thomas T, Castranova V, & Demokritou P (2014). Development and characterization of an exposure platform suitable for physico-chemical, morphological and toxicological characterization of printer-emitted particles (PEPs). Inhal Toxicol, 26(7), 400–408. [PubMed: 24862974]

Pyrgiotakis G, McDevitt J, Bordini A, Diaz E, Molina R, Watson C, Deloid G, Lenard S, Fix N, & Mizuyama Y (2014). A chemical free, nanotechnology-based method for airborne bacterial inactivation using engineered water nanostructures. Environmental Science: Nano, 1(1), 15–26.

Ramos K, Ramos L, & Gómez-Gómez MM (2017). Simultaneous characterisation of silver nanoparticles and determination of dissolved silver in chicken meat subjected to in vitro human gastrointestinal digestion using single particle inductively coupled plasma mass spectrometry. Food chemistry, 221, 822–828. [PubMed: 27979280]

Rizvi SSH (1995). In Rao MA & Rizvi SSH (Eds.), Engineering properties of foods. In: Academic Press, New York.

Schasteen CS, Wu J, Schulz MG, & Parsons CM (2007). Correlation of an immobilized digestive enzyme assay with poultry true amino acid digestibility for soybean meal. Poultry science, 86(2), 343–348.

Sekhon BS (2010). Food nanotechnology–an overview. Nanotechnology, science and applications, 3, 1.

Servin AD, & White JC (2016). Nanotechnology in agriculture: next steps for understanding engineered nanoparticle exposure and risk. NanoImpact, 1, 9–12.

Šimon P, & Joner E (2008). Conceivable interactions of biopersistent nanoparticles with food matrix and living systems following from their physicochemical properties. Journal of Food & Nutrition Research, 47(2).

Singh S, & Nalwa HS (2007). Nanotechnology and health safety - Toxicity and risk assessments of nanostructured materials on human health. Journal of Nanoscience and Nanotechnology, 7(9), 3048–3070. [PubMed: 18019130]

Smolkova B, El Yamani N, Collins AR, Gutleb AC, & Dusinska M (2015). Nanoparticles in food. Epigenetic changes induced by nanomaterials and possible impact on health. Food and Chemical Toxicology, 77, 64–73. [PubMed: 25554528]

Sohal IS, O'Fallon KS, Gaines P, Demokritou P, & Bello D (2018). Ingested engineered nanomaterials: state of science in nanotoxicity testing and future research needs. Part Fibre Toxicol, 15(1), 29. [PubMed: 29970114]

Sopade PA, & Gidley MJ (2009). A rapid in vitro digestibility assay based on glucometry for investigating kinetics of starch digestion. Starch Stärke, 61(5), 245–255.

Surh J, Decker EA, & McClements DJ (2006). Influence of pH and pectin type on properties and stability of sodium-caseinate stabilized oil-in-water emulsions. Food Hydrocolloids, 20(5), 607–618.

Versantvoort CHM, Oomen AG, Van de Kamp E, Rompelberg CJM, & Sips A (2005). Applicability of an in vitro digestion model in assessing the bioaccessibility of mycotoxins from food. Food and Chemical Toxicology, 43(1), 31–40. [PubMed: 15582193]

Walczak AP, Kramer E, Hendriksen PJM, Helsdingen R, van der Zande M, Rietjens IMCM, & Bouwmeester H (2015). In vitro gastrointestinal digestion increases the translocation of polystyrene nanoparticles in an in vitro intestinal co-culture model. Nanotoxicology, 9(7), 886–894. [PubMed: 25672814]

Weir A, Westerhoff P, Fabricius L, Hristovski K, & Von Goetz N (2012). Titanium dioxide nanoparticles in food and personal care products. Environmental science & technology, 46(4), 2242–2250. [PubMed: 22260395]

Yi L, Van Boekel MAJS, Boeren S, & Lakemond CMM (2016). Protein identification and in vitro digestion of fractions from Tenebrio molitor. European Food Research and Technology, 242(8), 1285–1297.

Zhang C, Li Y, Liu L, Gong Y, Xie Y, & Cao Y (2018). Chemical Structures of Polyphenols That Critically Influence the Toxicity of ZnO Nanoparticles. Journal of agricultural and food chemistry, 66(7), 1714–1722. [PubMed: 29383937]

Zhang R, Zhang Z, Zhang H, Decker EA, & McClements DJ (2015). Influence of emulsifier type on gastrointestinal fate of oil-in-water emulsions containing anionic dietary fiber (pectin). Food Hydrocolloids, 45, 175–185.

Zhang Z, Song H, Peng Z, Luo Q, Ming J, & Zhao G (2012). Characterization of stipe and cap powders of mushroom (Lentinus edodes) prepared by different grinding methods. Journal of Food Engineering, 109(3), 406–413.

Zhang Z, Zhang R, Zou L, & McClements DJ (2016). Tailoring lipid digestion profiles using combined delivery systems: mixtures of nanoemulsions and filled hydrogel beads. RSC Advances, 6(70), 65631–65637.

Zhao X, Ao Q, Du F, Zhu J, & Liu J (2010). Surface characterization of ginger powder examined by X-ray photoelectron spectroscopy and scanning electron microscopy. Colloids and Surfaces B: Biointerfaces, 79(2), 494–500. [PubMed: 20605705]

(a)

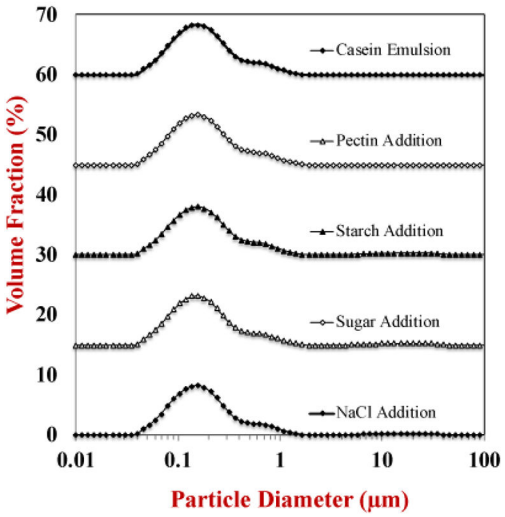

(b)

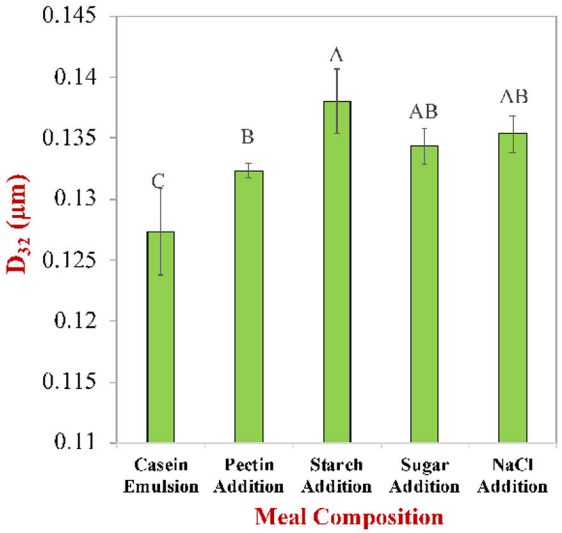

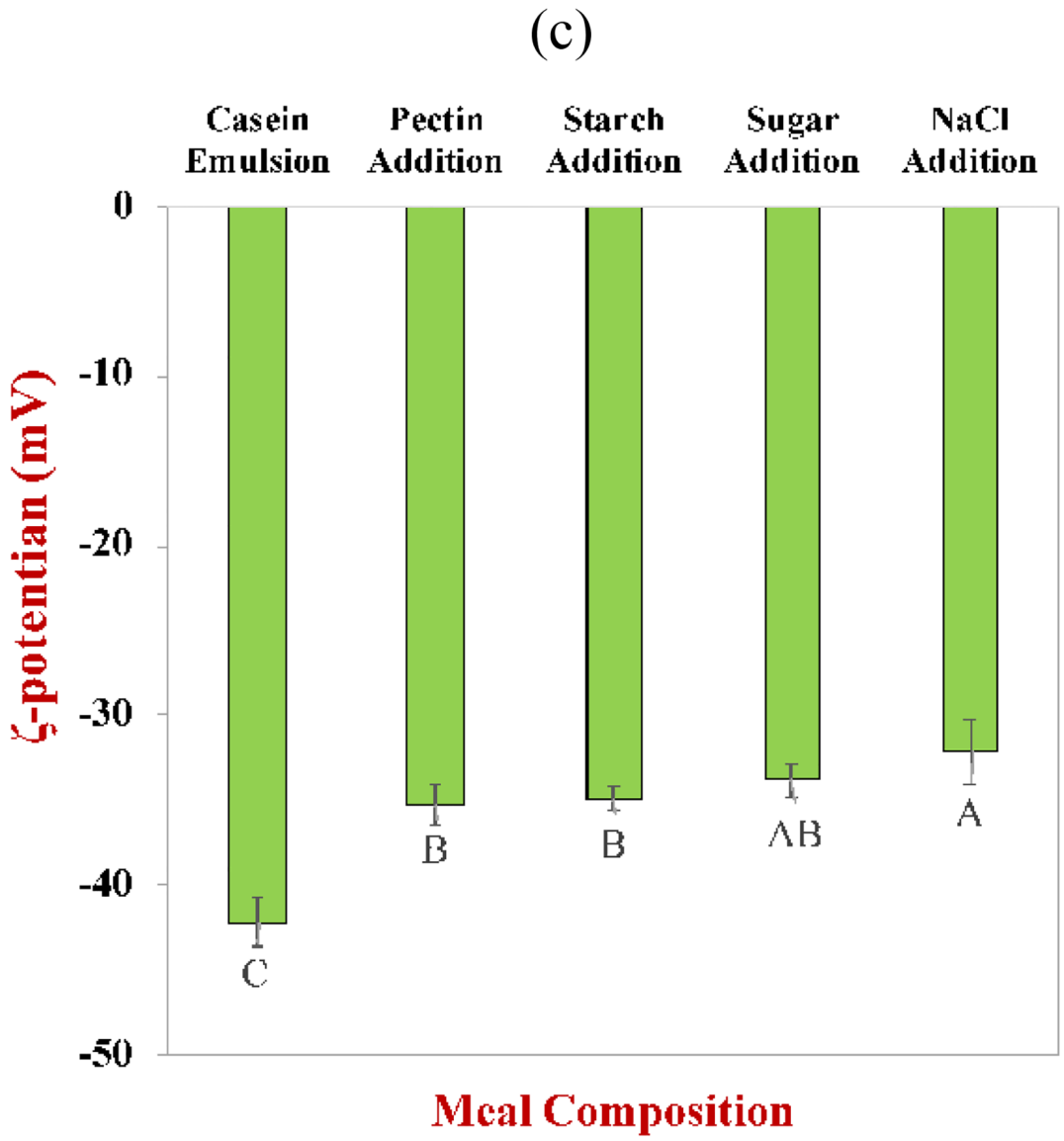

Figure 1.

The particle size distribution (a), mean particle diameter (b), and electrical characteristics (c) of the particles in the standard meal after sequentially adding different components.

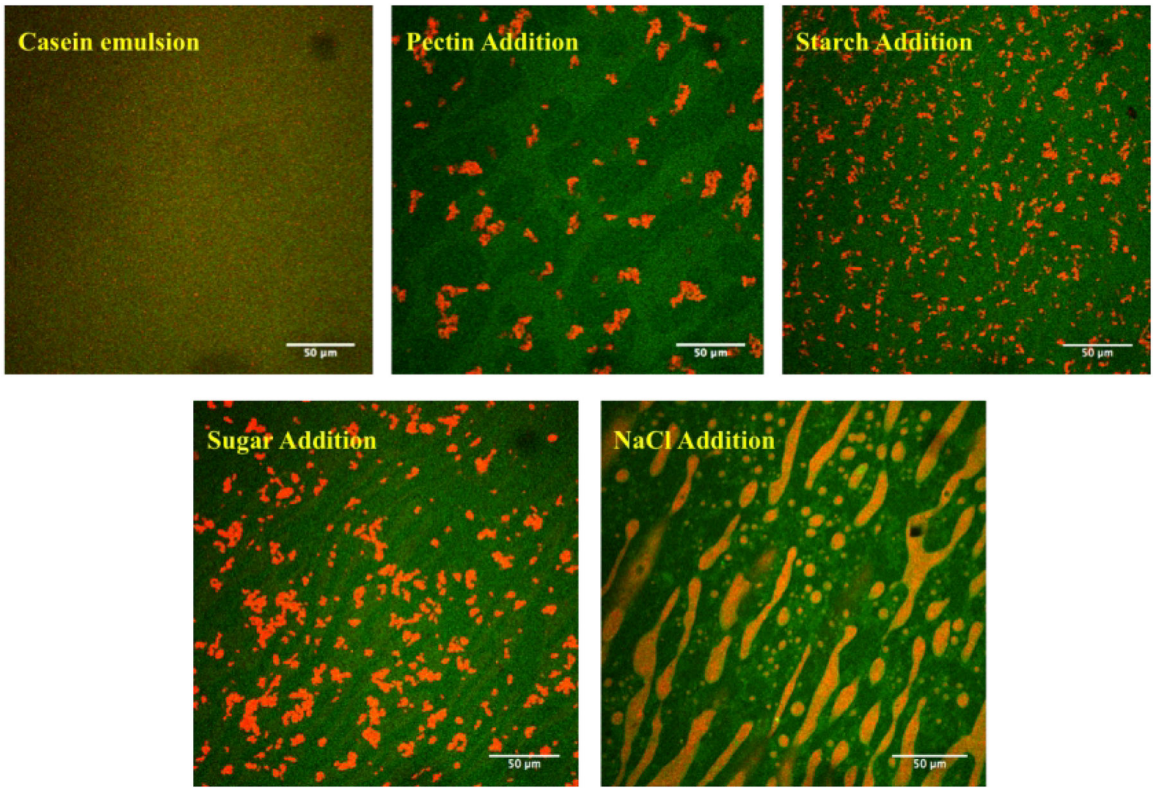

Figure 2.

Confocal microscopy images of standard meals after sequential addition of different components during its fabrication. The oil phase (red) was stained with Nile red and the protein phase (green) was stained by FITC. The scale bars are 50 μm.

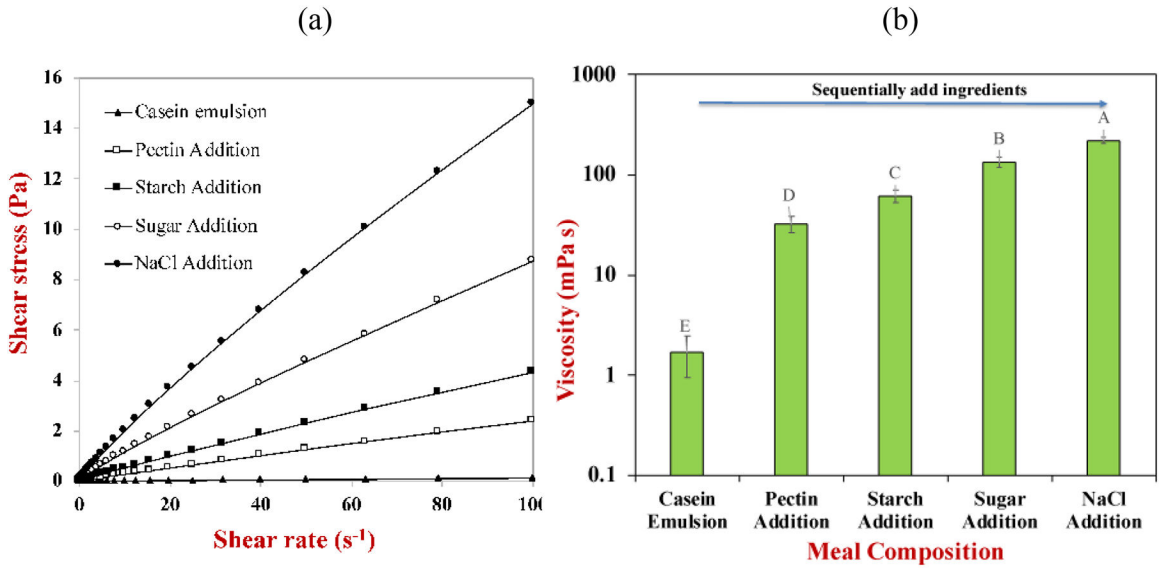

Figure 3.

The apparent shear viscosity of standard meal after sequential addition of different components to the base oil-in-water emulsion: (a) shear stress *versus* shear rate profiles; (b) average apparent shear viscosity (from 10 to 100 s^{-1}).

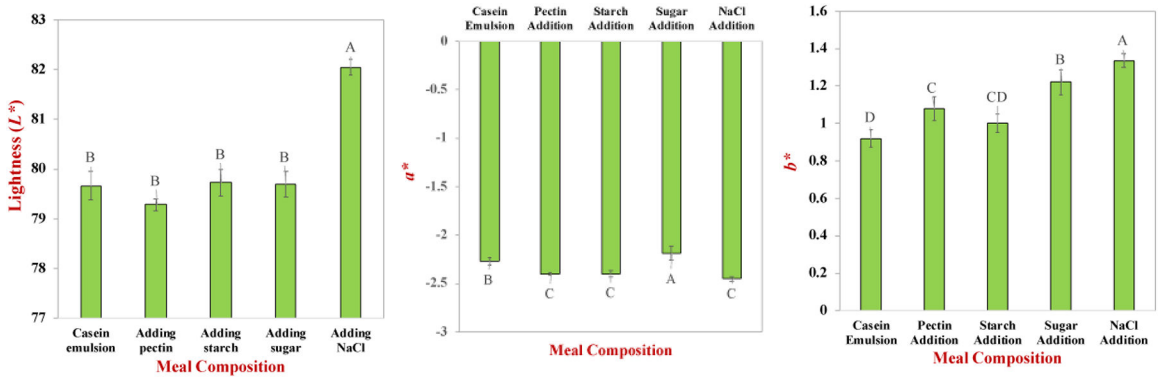

Figure 4.

The tristimulus color coordinates (*L*, a*, b**) of standard meals after addition of each component during its fabrication.

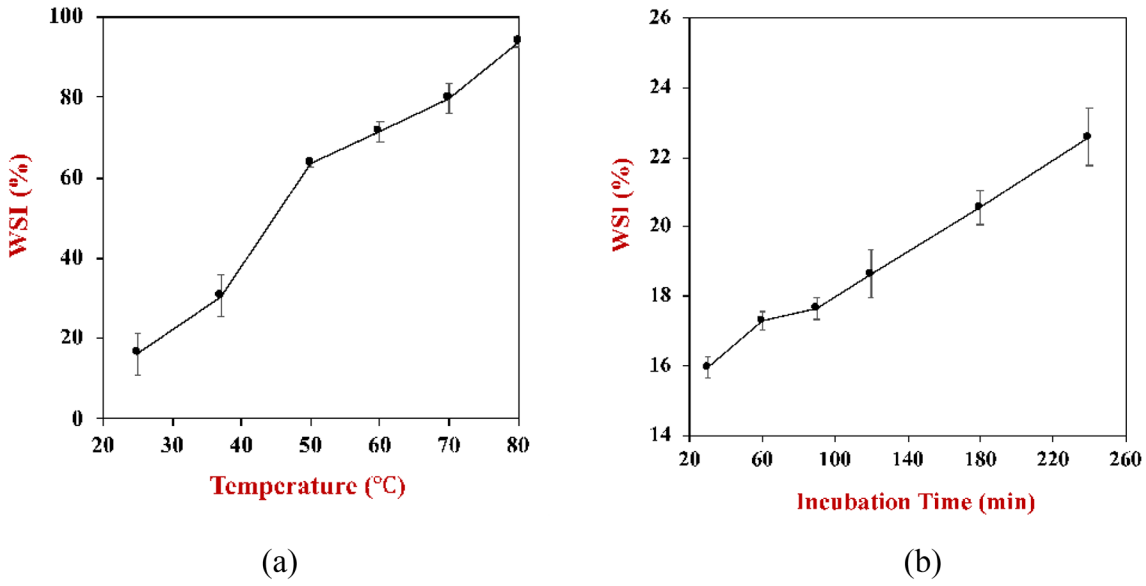

(a) (b)

Figure 5.

The water solubility index (WSI) of standard meal powder after exposure to different treatments: (a) storage temperatures for 30 min; (b) incubation times at 25 °C.

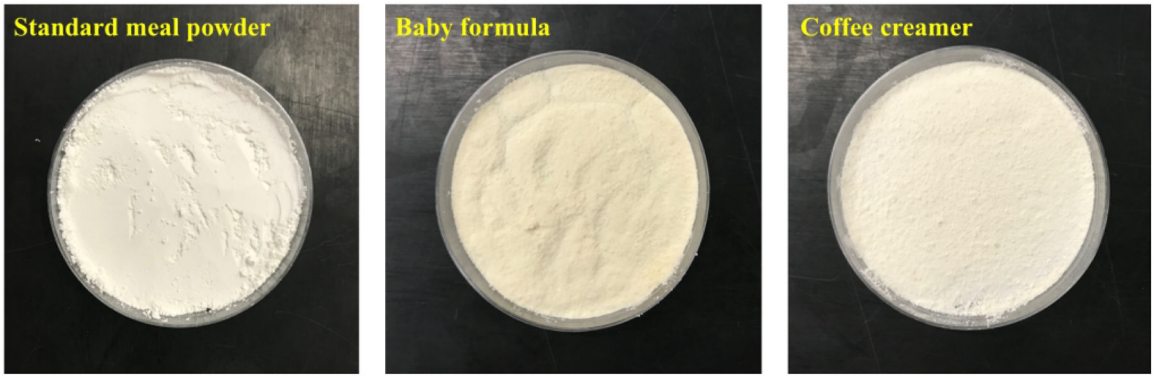

Figure 6.

The optical images of standard meal powder compared to other commercial powder products (i.e., baby formula and coffee creamer).

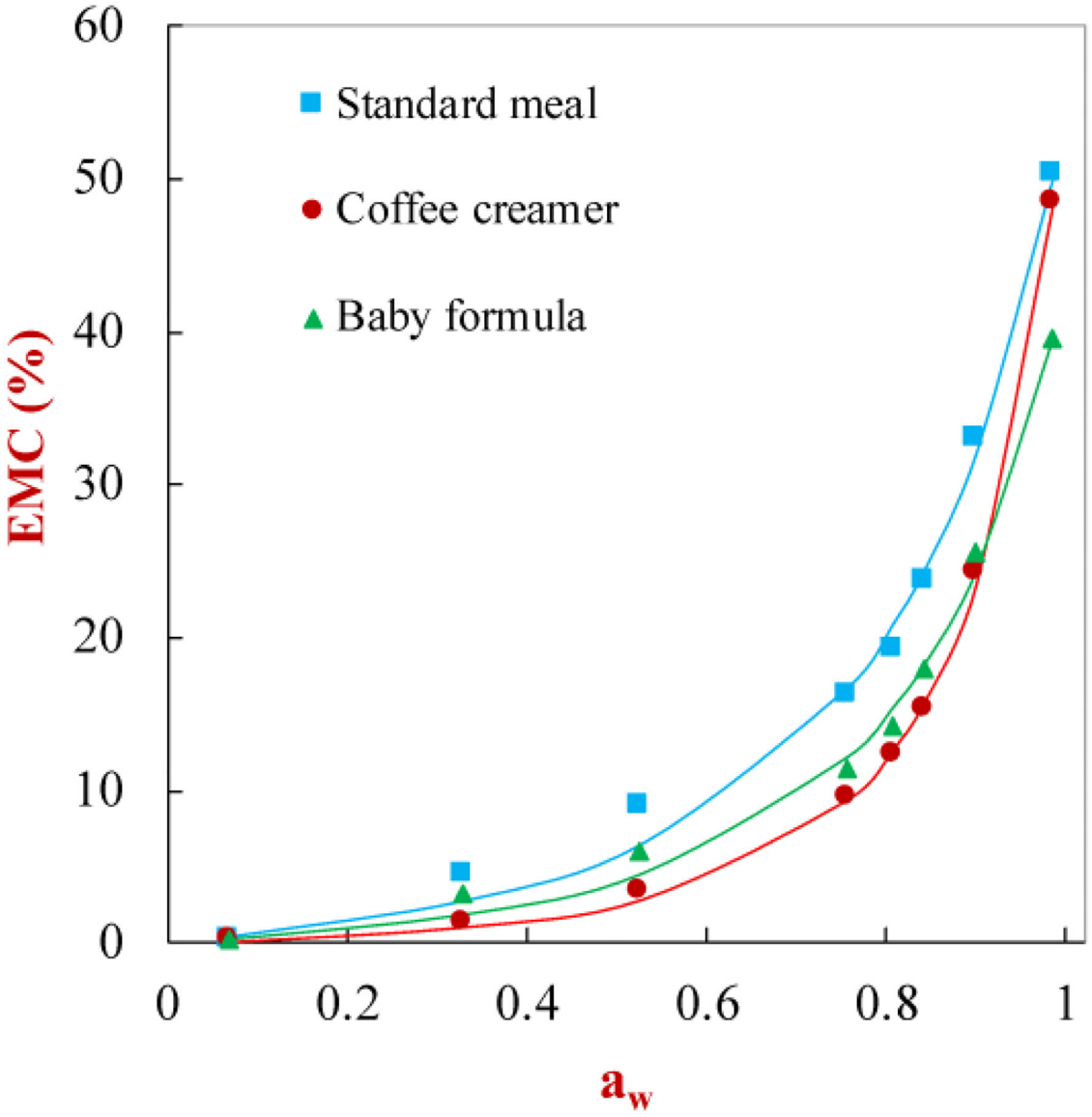

Figure 7.

The moisture sorption isotherm characteristics of standard meal powder and other commercial powder products (i.e., baby formula and coffee creamer). The points are experimental data, while the lines are predictions made using the Guggenheim-Anderson-De Boer Model.

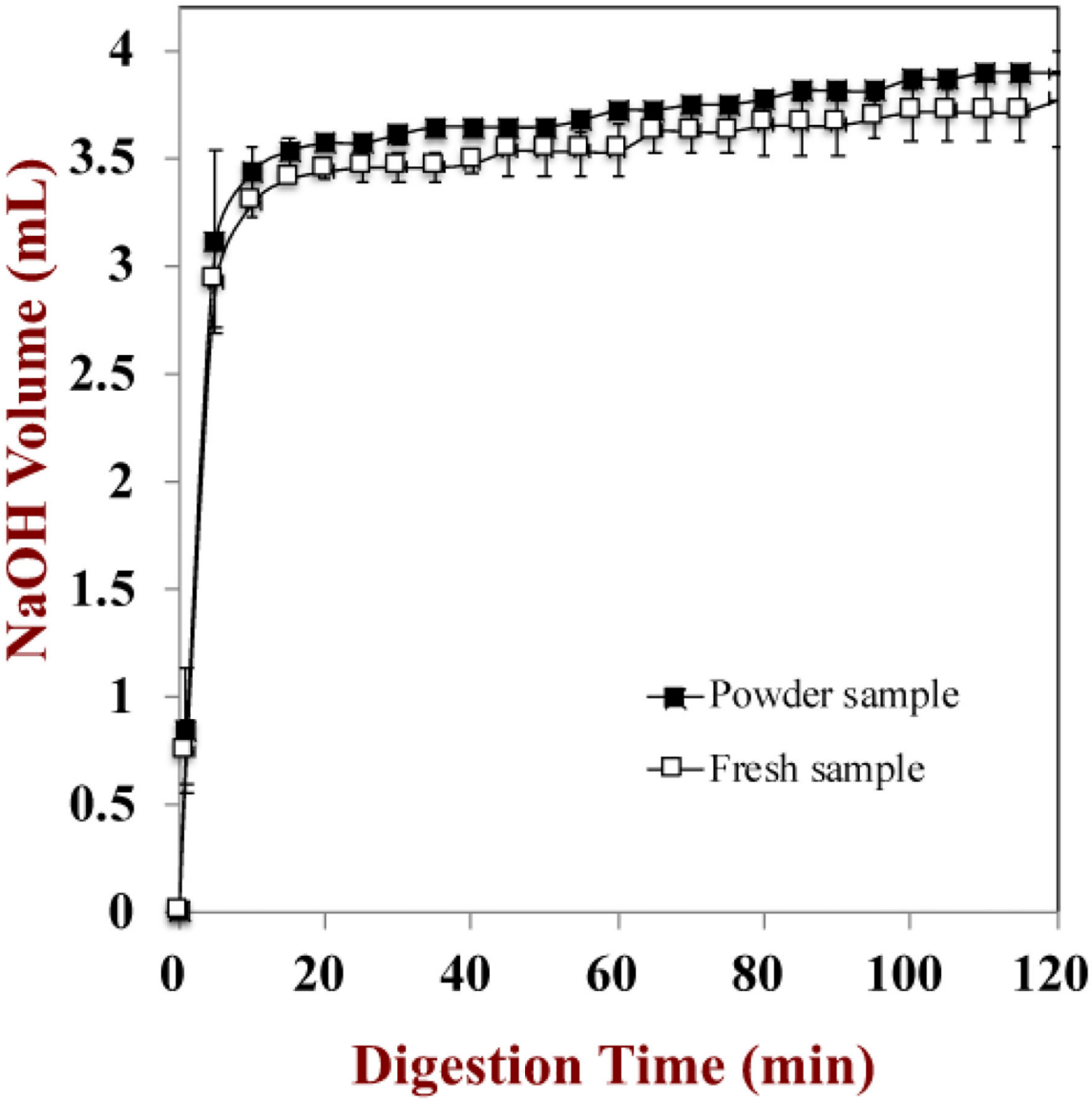

Figure 8.
The digestion properties of the fresh and reconstituted standard meal: the amount of NaOH required to keep the pH constant during the small intestine phase was measured.

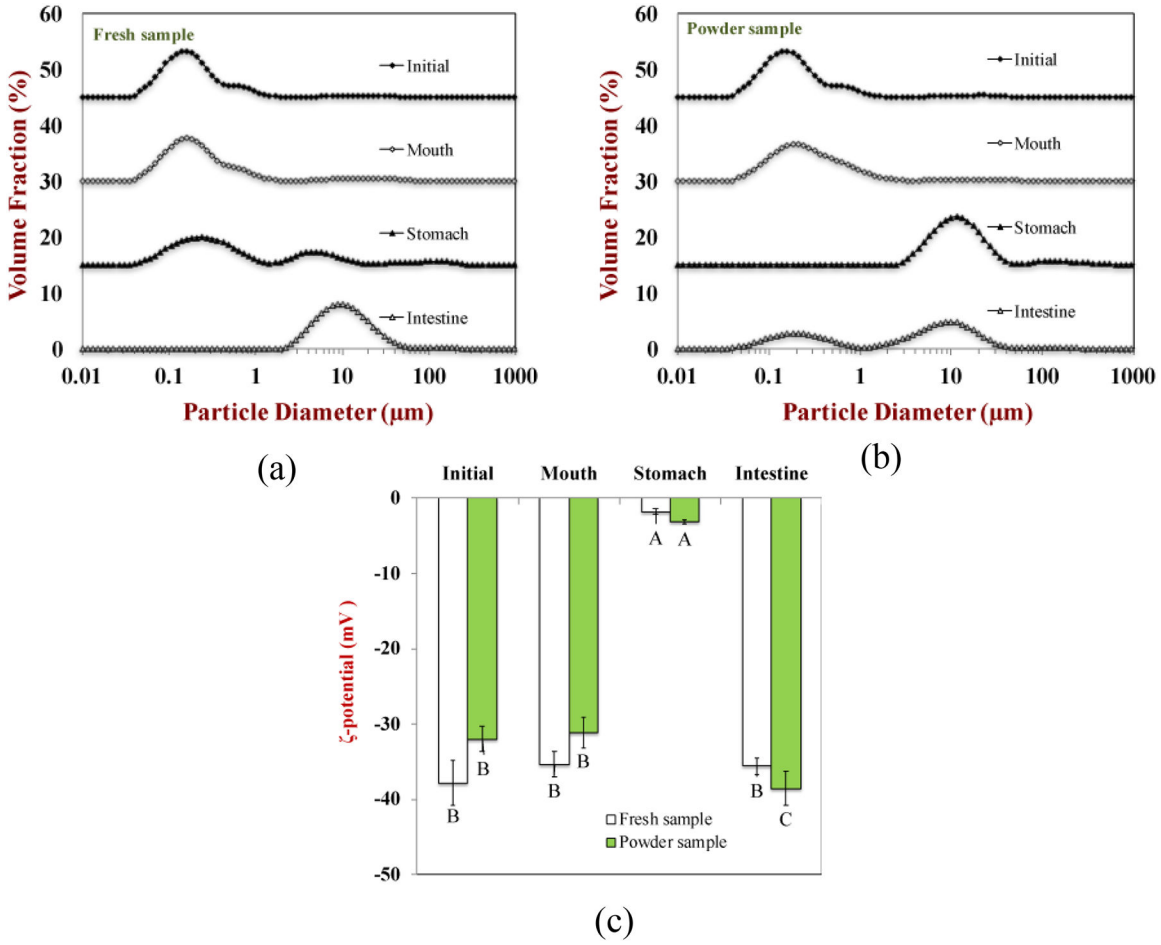

Figure 9.

The particle size and charge properties of standard meal solution and powder sample (after restore) during different steps of digestion process.

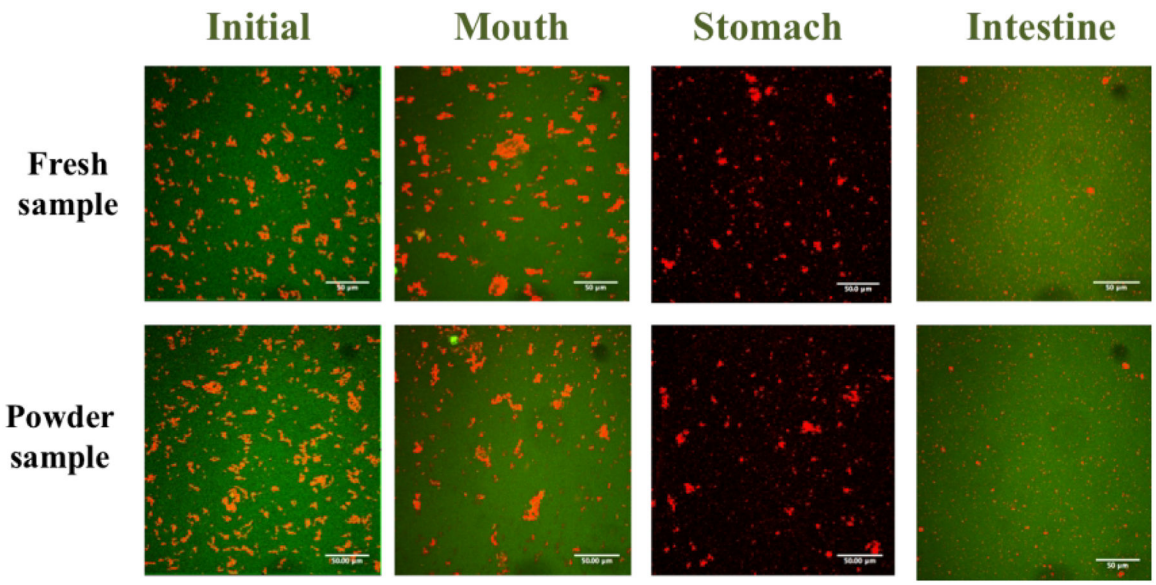

Figure 10.

The confocal micrographs of standard meal solution and powder sample (after restore) during different steps of digestion process, the oil phase (red) was stained with Nile red and the protein phase (green) was stained by FITC. The scale bars are 50 μm.

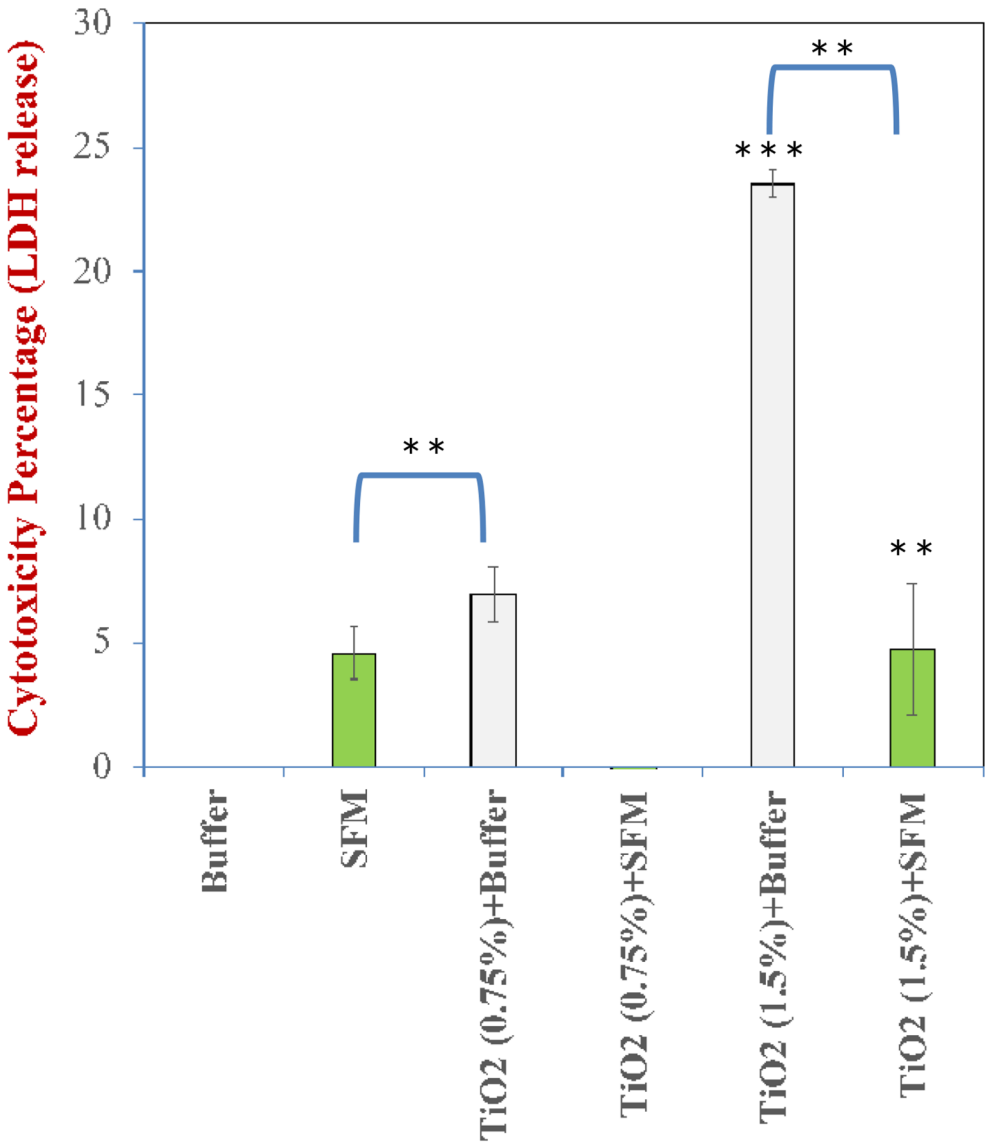

Figure 11.

Cytotoxicity assessment of standardized food model (SFM) and fasting medium (phosphate buffer) digestae against a model gut epithelium. TiO_2 particles are significantly less cytotoxic in the presence of SFM, suggesting that food matrix effects have an important impact on the biological activity of ingested nanomaterials. $p = 0.01$ **, $p < 0.001$ ***

Table 1:

The formulation of standard food matrix based on the survey of the typical US diet (www.ars.usda.gov/nea/bhnrc/fsrg).

Component	Level (g/100g)
Protein (Sodium caseinate)	3.44
Sugar (Sucrose)	4.57
Dietary Fiber (Pectin)	0.70
Starch (Corn starch)	5.15
Fat (Corn oil)	3.42
Minerals (Sodium chloride)	0.534

Table 2.

The particle characteristics of powdered standard meal and two commercial food powders (baby formula and coffee creamer). Different letters in the same row indicate the samples are statistically different ($p < 0.05$).

Parameters	**Powders**		
	Standard meal powder	**Baby formula**	**Coffee creamer**
Repose angle (°)	27.87 ± 0.48[a]	38.5 ± 1.39[b]	26.71 ± 1.46[a]
Slide angle (°)	28.22 ± 2.14[a]	53.12 ± 5.95[b]	24.34 ± 0.88[a]
Bulk density (g/mL)	0.48 ± 0.02[a]	0.39 ± 0.01[b]	0.24 ± 0.01[c]
*L**	94.19 ± 0.09[a]	87.10 ± 0.01[b]	90.7 ± 0.09[c]
*a**	−0.26 ± 0.02[a]	0.78 ± 0.19[b]	0.35 ± 0.02[c]
*b**	3.04 ± 0.05[a]	17.26 ± 0.39[b]	8.87± 0.05[c]

Table 3.

The nonlinear regression parameters obtained by fitting the GAB model to the moisture content data for the different powders.

Parameters	Powders		
	Standard meal powder	Baby formula	Coffee creamer
X_0	476.4	388.2	268.8
C	0.01	0.01	0.01
K	0.71	0.73	0.83
R^2	0.954	0.967	0.991